Advances and Applications in Fluid Mechanics

Published Online: December 2014
Available online at http://pphmj.com/journals/aafm.htm
Volume 17, Number 1, 2015, Pages 91-114 **ISSN: 0973-4686**

NUMERICAL SIMULATION OF BUBBLY FLOW BY AN IMPROVED VORTEX IN CELL METHOD

Tomomi Uchiyama*, Yutaro Yoshii, Bin Chen and Zhiwei Wang

EcoTopia Science Institute
Nagoya University
Furo-cho, Chikusa-ku, Nagoya 464-8601, Japan
e-mail: uchiyama@is.nagoya-u.ac.jp

Software Cradle Co., Ltd.
3-4-5, Umeda, Kita-ku, Osaka 530-0001, Japan

State Key Laboratory of Multiphase Flow in Power Engineering
Xi'an Jiaotong University
Xi'an 710049, P. R. China

Shenzhen Institutes of Advanced Technology
Chinese Academy of Sciences
Xueyuan Avenue 1068
Shenzhen 518035, P. R. China

Abstract

A simulation method for gas-liquid bubbly flows entraining small bubbles is proposed. It is based on the Vortex in Cell (VIC) method originally presented to simulate incompressible single-phase flows. The staggered grid discretization method and the vorticity correction method, which were proposed for the VIC method simulating single-

Received: June 17, 2014; Accepted: July 10, 2014
2010 Mathematics Subject Classification: 76T10.
Keywords and phrases: gas-liquid two-phase flow, computational fluid dynamics. bubbly flow, bubble plume, vortex method.

*Corresponding author

phase flows by the authors' prior study, are employed. The liquid velocity field is discretized with vortex elements, and the time evolution of the bubbly flow is simulated by calculating the behavior of each vortex element and the bubble motion through the Lagrangian approach. The proposed method is applied to the simulation of a bubble plume in a water tank to discuss the validity and applicability. Small air bubbles are released successively from the base of the tank, and their rise due to the buoyant force induces the water flow around them. The simulation at the starting period of the bubble release highlights that the rising bubbles induce vortex rings at their top and that a bubble cluster appears owing to the entrainment of the bubbles into the vortex rings. The rising velocity of the top of the bubbles is proportional to the square-root of the flowrate of the released bubbles, being consistent with the existing theoretical and numerical investigations. The simulation also demonstrates that the developed bubble plume having jet characteristics is successfully captured.

Notations

B : side length of bubble-releasing square area

d : bubble diameter

$\boldsymbol{g}$: gravitational constant

p : pressure

Q : second invariant of the water velocity gradient tensor

t : time

t^* : nondimensional time $= t/(B/g)^{1/2}$

$\boldsymbol{u}$: velocity

u_{gt} : terminal velocity of bubble

U_p : rising velocity of plume top

U_1, U_2 : vertical components of water velocity on plume centerline

v : volume of single bubble $= \pi d^3/6$

W : redistribution function of vorticity

x, y, z : orthogonal coordinates

α : volume fraction

Δt : time increment

$\Delta x, \Delta y, \Delta z$: grid widths in directions of x, y, z

ν : kinematic viscosity

ρ : density

ϕ : scalar potential

$\boldsymbol{\psi}$: vector potential

$\boldsymbol{\omega}$: vorticity of liquid-phase $= \nabla \times \boldsymbol{u}_l$

Subscripts

0 : just above the bubble-releasing area

g : gas-phase

l : liquid-phase

x, y, z : components in directions of x, y, z

1. Introduction

Vortex in Cell (VIC) method was originally presented to simulate incompressible flows [1]. It is one of the vortex methods solving the vorticity equation. In the VIC method, the vorticity field is discretized with vortex elements, and the convection of each vortex element is traced by the Lagrangian approach to compute the time evolution of the flow. The Lagrangian calculation markedly reduces the numerical diffusion as well as ensures the higher numerical stability. Therefore, the VIC method is expected to be usefully employed for the direct numerical simulation (DNS) of

turbulent flows. The DNSs for developing free shear flows have been conducted [2-5]. But turbulent flows bounded by solid walls have been scarcely simulated by the VIC method.

The authors [6] have previously proposed two improvements of the VIC method. First, a staggered grid discretization method guarantees consistency among the discretized equations and prevents numerical oscillations in the solution. Second, a vorticity correction method enables the computation of vorticity fields satisfying the solenoidal condition. The VIC method in conjunction with the abovementioned two improvements, or the improved VIC method, was applied to the DNS of a turbulent channel flow [6]. The DNS highlighted the successful capture of the organized flow structures, such as streaks and streamwise vortices in the near wall region, demonstrating that the improved VIC method is applicable to DNS of wall turbulent flows. On the basis of the improved VIC method, one of the authors [7] also proposed a simulation method for incompressible gas flows laden with small solid particles. The method was favorably validated in simulations of small free falling solid particles in unbounded air [7]. Uchiyama and Shimada [8] used the method to simulate the interaction between a vortex pair and small solid particles near a horizontal wall in the air. The simulation made clear the agitation of particles by the vortex pair approaching the wall, the production of vorticity fields by the particles, and the particle-induced changes in the strength and behavior of the vortex pair.

Gas-liquid bubbly flows are observed in various engineering applications, such as heat exchangers, chemical reactors and waste treatment systems. As the dispersed bubbles interact closely with the liquid-phase, the bubbly flow simulation needs the simultaneous computation of the two phases. A number of simulation methods have been proposed [9]. Most of them use the Lagrangian-Eulerian approach, in which the bubble motion is traced by the Lagrangian calculation and the liquid flow is computed by grid-based methods such as finite difference method and finite volume method. One of the authors [10] proposed a simulation method for bubbly flows on the basis of the VIC method, which employs neither the staggered grid discretization nor the vorticity correction. In the method, the liquid vorticity

field is discretized with vortex elements, and the behavior of the vortex elements as well as the bubble motion is calculated by the Lagrangian approach. Thus, the method is based on the Lagrangian-Lagrangian approach. The method was applied to simulate a plane bubble plume [10], and it was confirmed that the simulated three-dimensional vortical flow induced by the rising bubbles agrees with the experimental result. Wang et al. [11] also employed the method for the simulation of an interaction between a plane bubble plume and a vortex ring, and they explored the effect of the bubbles on the behavior of the vortex ring.

The objective of this study is to propose again a simulation method for bubbly flows, which is based on the improved VIC method for single-phase flows presented in the authors' prior paper [6]. Both the staggered grid discretization and the vorticity correction are employed. The simulation of a bubble plume in a water tank, obtained by applying the proposed method, is also discussed to demonstrate the validity and applicability of the method.

2. Basic Equations and Numerical Method

2.1. Assumptions

The following assumptions are employed for the simulation:

(a) The mixture is a gas-liquid bubbly flow entraining small bubbles.

(b) Both phases are incompressible and no phase changes occur.

(c) The mass and momentum of the gas-phase are very small and negligible compared with those of the liquid-phase.

(d) The bubbles maintain their spherical shape, and neither fragmentation nor coalescence occurs.

2.2. Governing equations for bubbly flow

The mass conservation equation for the liquid-phase and that for the gas-phase is independently derived. Taking the summation of them and rearranging the resultant equation with the assumptions (a)-(c), the mass conservation equation for the two-phase mixtures is obtained [10]:

$$\frac{\partial \alpha_l}{\partial t} + \nabla \cdot (\alpha_l \boldsymbol{u}_l) = 0, \tag{1}$$

where $D\boldsymbol{u}_l/Dt = \partial \boldsymbol{u}_l/\partial t + (\boldsymbol{u}_l \cdot \nabla)\boldsymbol{u}_l$. The gas and liquid volume fractions α_g and α_l, respectively satisfy the following relation:

$$\alpha_g + \alpha_l = 1. \tag{2}$$

The momentum conservation equation for the two-phase mixtures, which is also derived from the equations for each phase by the same manner as the mass conservation equation, is expressed as [10]

$$\alpha_l \frac{D\boldsymbol{u}_l}{Dt} = -\frac{1}{\rho_l}\nabla p + \nu_l \nabla^2 \boldsymbol{u}_l + \alpha_l \boldsymbol{g}. \tag{3}$$

It is postulated that the virtual mass force, the drag force, the gravitational force, and the lift force act on the bubble. In this case, the equation of motion for the bubble is expressed by the following equation [12, 13] with the assumption (d):

$$\frac{d\boldsymbol{u}_g}{dt} = \frac{1 + C_V}{\beta + C_V}\frac{D\boldsymbol{u}_l}{Dt} - \frac{1}{\beta + C_V}\frac{3C_D}{4d}|\,\boldsymbol{u}_g - \boldsymbol{u}_l\,|(\boldsymbol{u}_g - \boldsymbol{u}_l)$$

$$+ \frac{\beta - 1}{\beta + C_V}\boldsymbol{g} - \frac{C_L}{\beta + C_V}(\boldsymbol{u}_g - \boldsymbol{u}_l) \times (\nabla \times \boldsymbol{u}_l), \tag{4}$$

where d is the bubble diameter, and β is the density ratio defined as ρ_g/ρ_l. C_V, C_D and C_L are the virtual mass coefficient, the drag coefficient, and the lift coefficient, respectively.

2.3. Vorticity equation and orthogonal decomposition of liquid velocity

When taking the curl of equation (3), the vorticity equation for the bubbly flow is derived:

$$\frac{\partial \boldsymbol{\omega}}{\partial t} + \nabla \cdot (\boldsymbol{\omega}\boldsymbol{u}_l) = \nabla \cdot (\boldsymbol{u}_l \boldsymbol{\omega}) + \frac{\nu_l}{\alpha_l}\nabla^2 \boldsymbol{\omega} + \frac{1}{\alpha_l}\nabla \alpha_l \times \left(\boldsymbol{g} - \frac{D\boldsymbol{u}_l}{Dt}\right), \tag{5}$$

where $\boldsymbol{\omega}$ is the vorticity of the liquid-phase.

$$\boldsymbol{\omega} = \nabla \times \boldsymbol{u}_l. \tag{6}$$

According to the Helmholtz theorem, any vector field can be represented as the summation of the gradient of a scalar potential ϕ and the curl of a vector potential $\boldsymbol{\psi}$. The liquid velocity $\boldsymbol{u}_l$ is thus expressed as

$$\boldsymbol{u}_l = \nabla\phi + \nabla \times \boldsymbol{\psi}. \tag{7}$$

The velocity calculated from equation (7) remains unaltered when any gradient of a scalar function is added to $\boldsymbol{\psi}$. To remove this arbitrariness, the following solenoidal condition is imposed on $\boldsymbol{\psi}$:

$$\nabla \cdot \boldsymbol{\psi} = 0. \tag{8}$$

When substituting equation (7) into equation (1), the following equation is obtained:

$$\frac{\partial \alpha_l}{\partial t} + \nabla \cdot [\alpha_l(\nabla\phi + \nabla \times \boldsymbol{\psi})] = 0. \tag{9}$$

Taking the curl of equation (7) and substituting equation (8) into the resultant equation, the following vector Poisson equation for $\boldsymbol{\psi}$ is derived:

$$\nabla^2\boldsymbol{\psi} = -\boldsymbol{\omega}. \tag{10}$$

3. Simulation Based on VIC Method

3.1. Discretization of vorticity field with vortex elements

Once ϕ and ψ have been computed from equations (9) and (10), respectively, the velocity $\boldsymbol{u}_l$ is calculated from equation (7). The vorticity $\boldsymbol{\omega}$ in equation (10) is estimated from equation (5). The VIC method discretizes the vorticity field with vortex elements and calculates the distribution of $\boldsymbol{\omega}$ by tracing the convection of each vortex element.

It is postulated that the position vector and vorticity for the vortex element p are $\boldsymbol{x}_p = (x_p, y_p, z_p)$ and $\boldsymbol{\omega}_p$, respectively. The Lagrangian

form of the vorticity equation, equation (5), is written as follows:

$$\frac{d\boldsymbol{x}_p}{dt} = \boldsymbol{u}_l, \tag{11}$$

$$\frac{d\boldsymbol{\omega}_p}{dt} = \nabla \cdot (\boldsymbol{u}_l \boldsymbol{\omega}) + \frac{\nu_l}{\alpha_l} \nabla^2 \boldsymbol{\omega} + \frac{1}{\alpha_l} \nabla \alpha_l \times \left(\boldsymbol{g} - \frac{D\boldsymbol{u}_l}{Dt} \right). \tag{12}$$

It is found from equation (12) that the vorticity varies with the passage of time due to the stretch-contraction of vortex element, the viscous diffusion, and the gradient of the phase distribution.

When the position and vorticity of a vortex element are known at time t, the values at $t + \Delta t$ are computed from equations (11) and (12). In the VIC method, the flow field is divided into computational grid cells to define $\boldsymbol{\psi}$, ϕ and $\boldsymbol{\omega}$ on the grids. If $\boldsymbol{\omega}$ is defined at a position $\boldsymbol{x}_k = (x_k, y_k, z_k)$, the vorticity $\boldsymbol{\omega}$ is assigned to $\boldsymbol{x}_k$, or a vortex element with vorticity $\boldsymbol{\omega}$ is redistributed onto $\boldsymbol{x}_k$.

$$\boldsymbol{\omega}(\boldsymbol{x}_k) = \sum_{p}^{N_v} \boldsymbol{\omega}_p W\left(\frac{x_k - x_p}{\Delta x} \right) W\left(\frac{y_k - y_p}{\Delta y} \right) W\left(\frac{z_k - z_p}{\Delta z} \right), \tag{13}$$

where N_v is the number of vortex elements, and Δx, Δy and Δz are the grid widths. For the redistribution function W, the following equation is employed [14]:

$$W(\varepsilon) = \begin{cases} 1 - 2.5\varepsilon^2 + 1.5|\varepsilon|^3, & |\varepsilon| < 1, \\ 0.5(2 - |\varepsilon|)^2(1 - |\varepsilon|), & 1 \le |\varepsilon| \le 2, \\ 0, & |\varepsilon| > 2. \end{cases} \tag{14}$$

3.2. Calculation of gas volume fraction

The abovementioned grid cells are also used to calculate the gas volume fraction α_g. It is supposed that a bubble with volume v exists in a grid cell. As the bubble diameter is small on the basis of the assumption (a), it is much

smaller than the grid cell width. The gas volume fraction in the grid cell α_g is given as:

$$\alpha_g = \frac{v}{\Delta x \Delta y \Delta z}. \tag{15}$$

The α_g value calculated from equation (15) remains unaltered even when the bubble moves within the grid cell, and it changes discontinuously from α_g to 0 when the bubble flows out the grid cell. To overcome these problems, the authors' prior study [10] computed α_g by the following method.

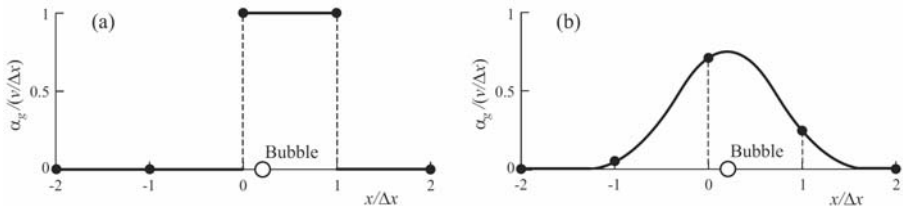

Figure 1. Calculation of gas volume fraction.

In the one-dimensional calculation, equation (15) yields $\alpha_g = v/\Delta x$. Defining α_g on the grid points, the grid points concerning to the grid cell involving the bubble take the α_g value, as shown in Figure 1(a). The present simulation computes the α_g value on the grid point q from the following equation:

$$\alpha_g(x_q) = \frac{v}{\Delta x} W_\alpha\left(\frac{x_q - x_g}{\Delta x}\right), \tag{16}$$

where x_g is the x-coordinate of the bubble position. For the function W_α, the following equation, which is the redistribution function of vortex element [14], is employed:

$$W_\alpha(\varepsilon) = \begin{cases} 0.5(|\varepsilon| + 1.5)^2 - 1.5(|\varepsilon| + 0.5)^2, & |\varepsilon| \le 0.5, \\ 0.5(-|\varepsilon| + 1.5)^2, & 0.5 \le |\varepsilon| \le 1.5, \\ 0, & |\varepsilon| > 1.5. \end{cases} \quad (17)$$

The distribution of α_g calculated from equation (16) is shown in Figure 1(b). α_g varies smoothly between the grid points around the bubble, and the relation $\int_{-\infty}^{\infty} W_\alpha \mathrm{d}x = 1$ is satisfied. These indicate that the continuity and conservation of α_g are indeed realized. The extension of equation (16) to the three-dimensional calculation gives the following equation:

$$\alpha_g(\boldsymbol{x}_q) = \frac{v}{\Delta x \Delta y \Delta z} W_\alpha\left(\frac{x_q - x_g}{\Delta x}\right) W_\alpha\left(\frac{y_q - y_g}{\Delta y}\right) W_\alpha\left(\frac{z_q - z_g}{\Delta z}\right). \quad (18)$$

Applying equation (18) to every bubble and taking the summation on each grid point, the α_g value on the grid point is obtained.

3.3. Discretization by staggered grid

For incompressible flow simulations, the MAC and SMAC methods solve the Poisson equation, which is derived from the equation for pressure gradient and the continuity equation. These methods employ a staggered grid to ensure consistency between the discretized equations, and to prevent numerical oscillations of the solution. The staggered grid would appear to be indispensable for discretizing the Poisson equation for ψ and the Laplace equation for ϕ, which are derived in the VIC method. However, staggered grids are not readily accommodated in the existing VIC method.

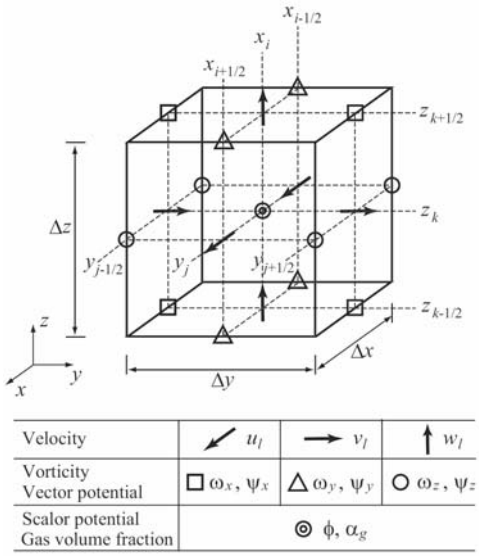

Figure 2. Computational grid and computed variables.

The authors demonstrated that VIC methods are applicable to simulations of single-phase flows [6] and particle-laden gas flows [7, 8], which use staggered grids. The current simulation employs the staggered grid as illustrated in Figure 2. The scalar potential ϕ and the gas volume fraction α_g are defined at the center of a grid cell. The liquid velocity $\boldsymbol{u}_l$ is defined at the sides, while the vorticity $\boldsymbol{\omega}$ and the vector potential $\boldsymbol{\psi}$ are defined on the edges.

3.4. Correction of vorticity

In the VIC method, the vorticity field is discretized with vortex elements, and the field is expressed by superimposing the vorticity distributions around each vortex element. The superposition is performed by equation (13). The resulting vorticity field $\boldsymbol{\omega}_r$ does not necessarily satisfy the solenoidal condition [14]. Denoting the vorticity satisfying this condition by $\boldsymbol{\omega}_s$ $(= \nabla \times \boldsymbol{u}_g)$, $\boldsymbol{\omega}_r$ is expressed as [4]

$$\boldsymbol{\omega}_r = \nabla F + \boldsymbol{\omega}_s, \tag{19}$$

where F is a scalar function. Equation (19) corresponds to the Helmholtz decomposition of $\boldsymbol{\omega}_r$.

Taking the divergence of equation (19), we obtain the Poisson equation for F:

$$\nabla^2 F = \nabla \cdot \boldsymbol{\omega}_r. \tag{20}$$

Calculating F from equation (20) and substituting into equation (19) gives the recalculated vorticity $\boldsymbol{\omega}_s$ [4]. This correction for vorticity needs to solve the Poisson equation, which increases the computational time. To reduce this additional cost, the authors [6] have proposed a simplified correction method.

The uncorrected vorticity, $\boldsymbol{\omega}_r$, is linked to $\boldsymbol{\psi}_r$ through equation (10). Taking the divergence of equation (10) and substituting equation (20) into the resultant equation, the following relations are obtained:

$$\begin{aligned} \nabla^2(\nabla \cdot \boldsymbol{\psi}_r) &= -\nabla \cdot \boldsymbol{\omega}_r \\ &= -\nabla^2 F. \end{aligned} \tag{21}$$

Unlike equation (8), which assumes the solenoidal condition for $\boldsymbol{\psi}$, the following equation for a non-solenoidal vorticity is derived from equation (21):

$$\nabla \cdot \boldsymbol{\psi}_r = -F. \tag{22}$$

Using $\boldsymbol{\omega}_r$ to calculate $\boldsymbol{\psi}_r$ from equation (10), and determining ϕ_r from equation (9), the curl of $\boldsymbol{u}_r$ transforms as follows:

$$\begin{aligned} \nabla \times \boldsymbol{u}_r &= \nabla \times (\nabla \phi_r + \nabla \times \boldsymbol{\psi}_r) \\ &= \nabla(\nabla \cdot \boldsymbol{\psi}_r) - \nabla^2 \boldsymbol{\psi}_r \\ &= -\nabla F + \boldsymbol{\omega}_r \\ &= \boldsymbol{\omega}_s. \end{aligned} \tag{23}$$

Equation (23) demonstrates that the curl of the velocity $\boldsymbol{u}_r$ calculated from $\boldsymbol{\omega}_r$ yields a vorticity $\boldsymbol{\omega}_s$ that satisfies the solenoidal condition. If the vorticity is recalculated by equation (23), or the vorticity is corrected immediately after calculating the liquid velocity by equation (7), the discretization error in the vorticity is completely removed and the flow dynamics are accurately simulated without solving the Poisson equation (equation (20)). It should be noted that the staggered grid is required for rendering the transformation in equation (23) applicable to the corresponding discretized equations.

3.5. Numerical procedure

Given the flow at time t, the flow at $t + \Delta t$ is simulated by the following procedure:

(1) Calculate the bubble motion from equation (4).

(2) Calculate α_g from equation (18), and compute α_l from equation (2).

(3) Calculate the time variation of $\boldsymbol{\omega}$ at every grid point from equation (12).

(4) Calculate the convection of each vortex element from equation (11).

(5) Calculate $\boldsymbol{\omega}$ from equation (13).

(6) Calculate $\boldsymbol{\psi}$ from equation (10).

(7) Calculate ϕ from equation (9).

(8) Calculate $\boldsymbol{u}_l$ from equation (7).

(9) Correct the vorticity, or calculate the corrected vorticity from the curl of $\boldsymbol{u}_l$.

4. Application to Bubble Plume Simulation

4.1. Simulation conditions

The proposed method is applied to the simulation of a bubble plume to discuss the validity and the applicability. Murai and Matsumoto [15]

investigated the bubble plume with the numerical simulation as well as the experimental visualization. Figure 3 shows the flow configuration. Small air bubbles are released successively from a square area on the bottom of a water tank, and their rise due to the buoyant force induces the water flow around them, resulting in a bubble plume in the tank. The $x - y$ plane is horizontal, and the z-axis is taken in the vertically upward direction.

Table 1 lists the simulation conditions. The bubble-releasing area is square in shape, and the side length B is 25 mm. The horizontal cross-section of the tank is $4B \times 4B$, and the height of water is $16B$. The computational region $4B \times 4B \times 16B$ is divided into $40 \times 40 \times 160$ grid cells. In the VIC method for single-phase flow simulations, the conditions $\Delta t|\nabla u| < 1$ and $\Delta t\nu/h^2 < 1$ are needed for the stable computation, where h and u are the grid cell width and the velocity respectively. The time increment Δt in this simulation satisfies these CFL conditions.

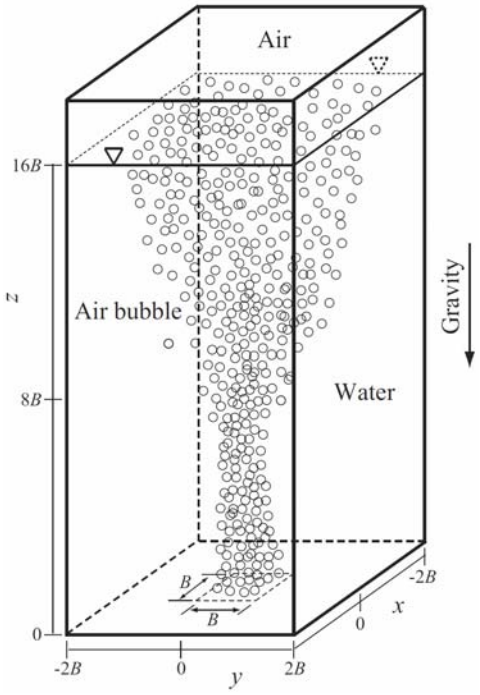

Figure 3. Configuration of bubble plume.

Table 1. Simulation conditions

Bubbly flow	Air/Water at 298 K
Side length of bubble-releasing area; B	25 mm
Horizontal cross-sectional area of water tank	$4B \times 4B$
Height of water	$16B$
Computational domain	$4B \times 4B \times 16B$
Number of grids	$40 \times 40 \times 160$
Mean diameter of bubble; d	0.4 mm
Gas volume fraction above bubble-releasing area; α_{g0}	0.005 - 0.03
Lift coefficient of bubble; C_L	0.5
Virtual mass coefficient of bubble; C_V	0.5
Time increment; Δt	4 ms

When releasing the bubbles from the square area, the velocity is set at zero. The releasing positions are determined by using random numbers. The bubble diameter d obeys the Gaussian distribution; the mean and the standard deviation are 0.4 mm and 0.04 mm, respectively. The virtual mass coefficient C_V and the lift coefficient C_L are 0.5. The drag coefficient C_D is given by the following equation:

$$C_D = \max\left\{\frac{48}{\mathrm{Re}_b}\left(1 - \frac{2.21}{\mathrm{Re}_b^{1/2}}\right), \frac{24}{\mathrm{Re}_b}\right\}, \tag{24}$$

where Re_b is the bubble Reynolds number defined as $d\,|\,\boldsymbol{u}_g - \boldsymbol{u}_l\,|/\nu_l$. Equation (24) combines the theoretical formula of Moore [16] and the Stokesian drag coefficient. It was also used in the simulation of Murai and Matsumoto [15].

The release of bubbles into the quiescent water commences at time $t^* = 0$. The water velocity thus at $t^* = 0$ is zero.

On the tank wall, a non-slip condition is imposed. There exists no flow in the direction normal to the wall, and the relation of $\nabla \cdot \boldsymbol{\psi} = 0$ is satisfied.

Therefore, the tangential component of $\boldsymbol{\psi}$ is zero, and the gradient of the normal component in the direction normal to the wall is also zero. The boundary condition of $\boldsymbol{\omega}$ is given by the curl of the velocity. On the walls at $y = \pm 2B$, for example, these boundary conditions are expressed as:

$$\boldsymbol{u}_l = 0, \tag{25}$$

$$\frac{\partial \phi}{\partial y} = 0, \tag{26}$$

$$\psi_x = 0, \quad \psi_z = 0, \quad \frac{\partial \psi_y}{\partial y} = 0, \tag{27}$$

$$\omega_x = \frac{\partial u_{lz}}{\partial y}, \quad \omega_y = 0, \quad \omega_z = -\frac{\partial u_{lx}}{\partial y}. \tag{28}$$

The upper boundary corresponds to the free-surface. In this simulation, the deformation is ignored, and the velocity gradient normal to the boundary is set at zero:

$$\frac{\partial^2 \phi}{\partial z^2} = 0, \tag{29}$$

$$\frac{\partial \psi_x}{\partial z} = 0, \quad \frac{\partial \psi_y}{\partial z} = 0, \quad \frac{\partial \psi_z}{\partial z} = -\frac{\partial \psi_x}{\partial x} - \frac{\partial \psi_y}{\partial y}. \tag{30}$$

Equations (9) and (10) are solved by the successive over-relaxation (SOR) method.

4.2. Simulation results

Figure 4 shows the temporal evolution of the bubble distribution after starting the bubble release at time $t = 0$. The gas volume fraction just above the bubble-releasing area α_{g0} is 0.02. The bubbles, rising vertically in the quiescent water due to the buoyant force, form a cluster of a mushroom shape at their top just after their release $(t^* = 40)$. This is because the rising bubbles induce vortex rings of the water, and accordingly they are entrained

into the vortex rings, as explained later. Such bubble cluster is known to appear in the starting period of bubble plumes. Murai and Matsumoto [15] grasped the similar bubble cluster, and Caballina et al. [17] also reported such bubble cluster in a simulation of a plane bubble plume. At $t^* = 80$ and 120, the bubble cluster rises in the water. When $t^* \geq 200$, the bubbles rise almost vertically until $z = 6B$, and they disperse markedly in the horizontal direction at $z > 6B$. A fully-developed bubble plume occurs.

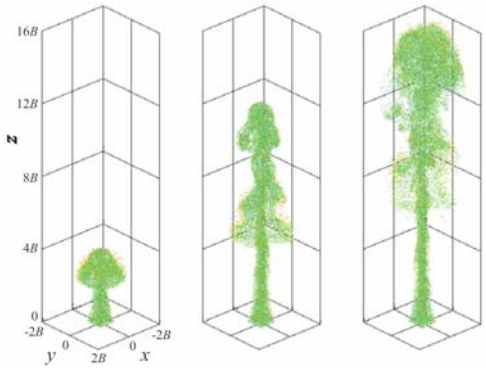

(a) $t^* = 40$ (b) $t^* = 80$ (c) $t^* = 120$

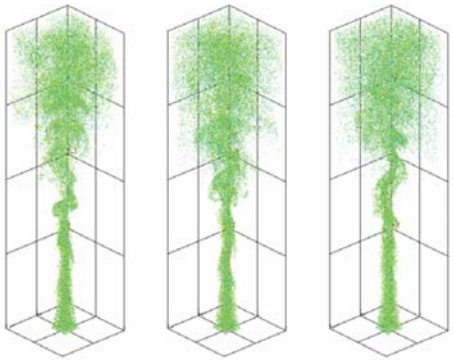

(d) $t^* = 200$ (e) $t^* = 280$ (f) $t^* = 400$

Figure 4. Temporal evolution of bubble distribution $(\alpha_{g0} = 0.02)$.

The rising velocity of the top of the plume is larger than the terminal velocity of a bubble u_{gt} in quiescent water. This is because it is affected by

the upward water flow induced by the rising bubbles. According to the dimension analysis of Caballina et al. [17], the rising velocity of plume top U_p is proportional to the square-root of the flowrate of the released bubbles Q_g. Figure 5 shows the relation between $U_p/(gB)^{1/2}$ and α_{g0}. U_p increases with α_{g0}, satisfying the relation of $U_p \propto \alpha_{g0}^{1/2}$. It is discovered that the present result is parallel with the analysis of Caballina et al. in due consideration of the relation $\alpha_{g0} \propto Q_g$.

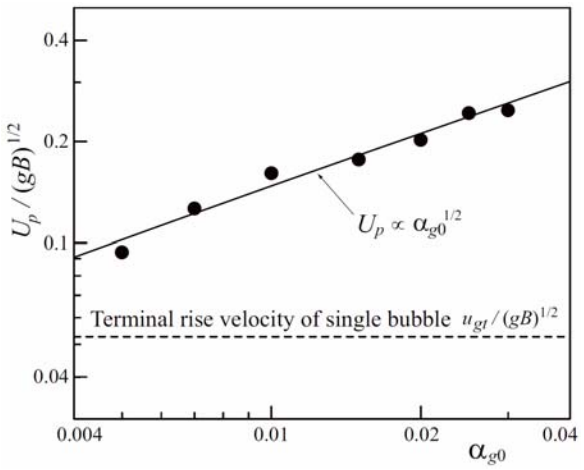

Figure 5. Rising velocity of starting plume.

Trying to apply the simulation method proposed in the authors' prior study [10], the results were the same as those obtained by the present method in the case of $\alpha_{g0} \leq 0.015$. But the simulation for $\alpha_{g0} \geq 0.02$ collapsed at a time step just before the appearance of the fully-developed plume. This may be attributable to the fact that the solenoidal condition of the vorticity field is not exactly satisfied. The present method is applicable to the simulation even at $\alpha_{g0} = 0.03$ as demonstrated in Figure 5, expanding successfully the simulation condition of α_{g0}.

To grasp the water flow induced by the rising bubbles, the velocity distribution on the central vertical cross-section is plotted in Figure 6. The

distributions at the time points indicated in Figure 4 are depicted. When $t^* \leq 120$, the upward flow is induced around the centerline, and eddies with various scales appear around the rising bubble cluster. At $t^* \geq 200$, a core region exists on the centerline at $z \leq 6B$, and the velocity diffuses markedly in the horizontal direction at $z > 6B$. From these velocity distributions, one can find the appearance of a water flow having jet characteristics.

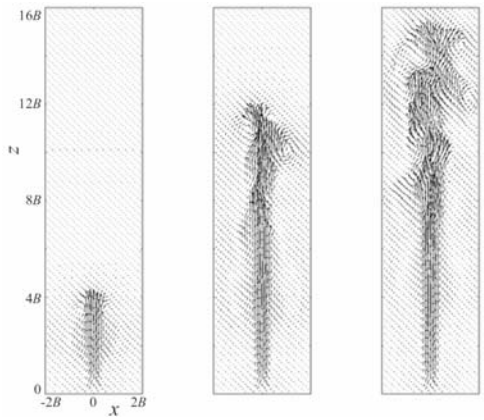

(a) $t^* = 40$ (b) $t^* = 80$ (c) $t^* = 120$

(d) $t^* = 200$ (e) $t^* = 280$ (f) $t^* = 400$

Figure 6. Temporal evolution of water velocity $(\alpha_{g0} = 0.02)$.

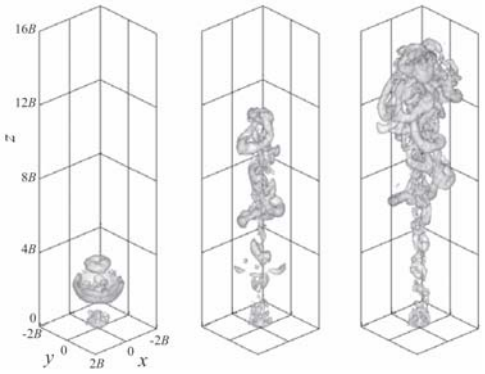

(a) $t^* = 40$ (b) $t^* = 80$ (c) $t^* = 120$

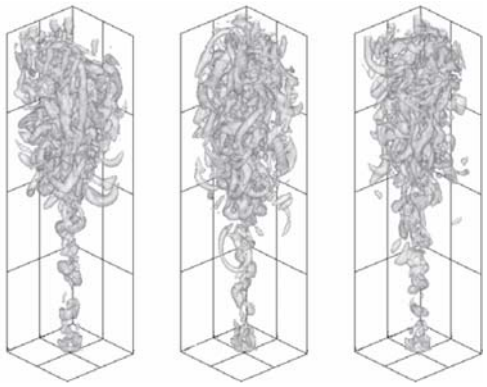

(d) $t^* = 200$ (e) $t^* = 280$ (f) $t^* = 400$

Figure 7. Temporal evolution of Q value $(\alpha_{g0} = 0.02,\ Q/(g/B) = 0.005)$.

Figure 7 shows the temporal evolution of the second invariant of the water velocity gradient tensor Q. The iso-surface of $Q/(g/B) = 0.005$ at six time points is presented. Q is defined by the following equation:

$$Q = \frac{1}{2}(W_{ij}W_{ij} - S_{ij}S_{ij}), \tag{31}$$

where the vorticity tensor W_{ij} and the deformation rate tensor S_{ij} are given as:

$$W_{ij} = \frac{1}{2}\left(\frac{\partial u_{li}}{\partial x_j} - \frac{\partial u_{lj}}{\partial x_i}\right), \quad S_{ij} = \frac{1}{2}\left(\frac{\partial u_{li}}{\partial x_j} + \frac{\partial u_{lj}}{\partial x_i}\right). \tag{32}$$

Vortex rings appear around the central axis at $t^* = 40$. The bubbles are entrained into the vortex rings, forming a bubble cluster as found in Figure 4. The vortex rings deform with the rise of the cluster, and eventually they change into three-dimensional vortex tubes. When $t^* \geq 200$, the entangled vortex tubes are visualized at $z \geq 8B$. One can grasp the vortical flow composed of the vortex tubes having various scales.

The iso-surfaces of the vertical component of the vorticity ω_z, $\omega_z/(B/g)^{1/2} = \pm 0.05$, are shown in Figure 8. Pairs of positive and negative vortex tubes exist and entangle in the developed region at $z \geq 8B$, indicating the appearance of a highly three-dimensional vortical flow.

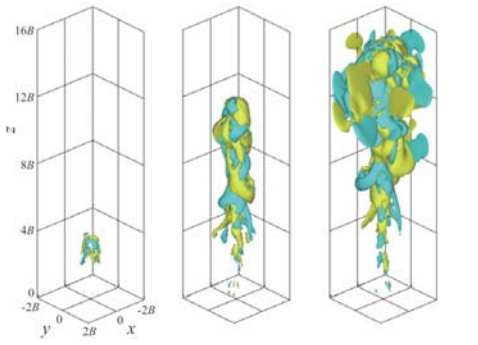

(a) $t^* = 40$ (b) $t^* = 80$ (c) $t^* = 120$

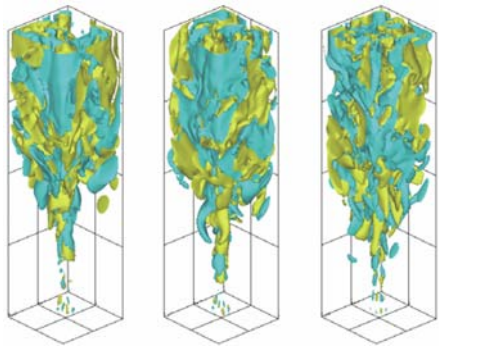

(d) $t^* = 200$ (e) $t^* = 280$ (f) $t^* = 400$

Figure 8. Temporal evolution of vertical component of vorticity ω_z ($\alpha_{g0} = 0.02$, $\omega_z/(B/g)^{1/2} = \pm 0.05$).

Figure 9 shows the time variation of the vertical component of the water velocity on the centerline, where $\alpha_{g0} = 0.02$. The variations of the velocities U_1 and U_2 at $z = 4B$ and $14B$, respectively, are plotted. The velocity U_2 is much lower than U_1. This indicates that the water momentum diffuses markedly in the horizontal direction in the fully-developed region, because U_1 and U_2 are computed in the core and fully-developed regions, respectively. It should also be noted that U_1 and U_2 fluctuate irregularly and that the amplitude and period of U_2 are much larger than those of U_1. This is attributable to the fact that U_2 is affected by the large-scale eddies existing in the fully-developed region.

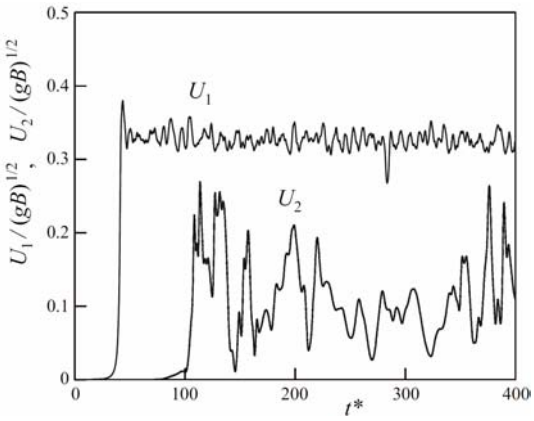

Figure 9. Time variation of vertical component of water velocity on plume centerline ($\alpha_{g0} = 0.02$).

5. Conclusions

A numerical simulation method for gas-liquid bubbly flows entraining small bubbles is proposed. It is based on the Vortex in Cell (VIC) method, of which numerical accuracy for single-phase flow simulation was successfully improved by the authors' prior study.

The proposed method is applied to the simulation of a bubble plume in a rectangular water tank to discuss the validity and the applicability. Small air

bubbles are released successively from a square area on the bottom of the tank, and their rise due to the buoyant force induces the water flow around them, resulting in the bubble plume in the tank. The simulation at the starting period of the bubble release highlights that the rising bubbles induce vortex rings at their top and that a bubble cluster of a mushroom shape appears owing to the entrainment of the bubbles into the vortex rings. This demonstrates that the proposed method can simulate the transient bubbly flow, which is known to occur in bubble plumes at the starting period. The simulation shows that the rising velocity of the top of the released bubbles is proportional to the square-root of the flowrate of the released bubbles. This is consistent with the existing theoretical analysis and numerical simulation. The simulation also demonstrates that the jet characteristics of the bubble plume, such as the existence of the core region just above the bubble-releasing area and the appearance of the three-dimensional vortical flow composed of eddies with various scales at the developed region, are favorably computed.

References

[1] J. P. Christiansen, Numerical simulation of hydrodynamics by the method of point vortices, J. Comput. Phys. 13 (1973), 363-379.

[2] G.-H. Cottet and P. Poncet, Advances in direct numerical simulations of 3D wall-bounded flows by vortex-in-cell methods, J. Comput. Phys. 193 (2003), 136-158.

[3] G. Winckelmans, R. Cocle, L. Dufresne and R. Capart, Vortex methods and their application to trailing wake vortex simulations, C. R. Physique 6 (2005), 467-486.

[4] R. Cocle, G. Winckelmans and G. Daeninck, Combining the vortex-in-cell and parallel fast multipole methods for efficient domain decomposition simulations, J. Comput. Phys. 227 (2008), 9091-9120.

[5] P. Chatelain, A. Curioni, M. Bergdorf, D. Rossinelli, W. Andreoni and P. Koumoutsakos, Billion vortex particle direct numerical simulations of aircraft wakes, Comput. Methods Appl. Mech. Engrg. 197 (2008), 1296-1304.

[6] T. Uchiyama, H. Hamada and Y. Yoshii, Direct numerical simulation of a turbulent channel flow by an improved vortex in cell method, International Journal of Numerical Methods for Heat and Fluid Flow 24 (2014), 103-123.

[7] T. Uchiyama, Numerical simulation of particle-laden gas flow by vortex in cell method, Powder Technology 235 (2013), 376-385.

[8] T. Uchiyama and S. Shimada, Numerical simulation of the interactions between a vortex pair and solid particles near a wall, Powder Technology 257 (2014), 55-67.

[9] C. Kleinstreuer, Two-phase Flow: Theory and Applications, Taylor & Francis, New York, 2003.

[10] T. Uchiyama and S. Matsumura, Three-dimensional vortex method for the simulation of bubbly flow, Trans. ASME, Journal of Fluids Engineering 132 (2010), 101402-1-101402-8.

[11] Z. Wang, T. Uchiyama and B. Chen, Numerical simulation of the interaction between vortex ring and bubble plume, Applied Mathematical Modelling 37 (2013), 10007-10026.

[12] T. R. Auton, J. C. R. Hunt and M. Prud'home, The force exerted on a body in inviscid unsteady non-uniform rotational flow, J. Fluid Mech. 197 (1988), 241-257.

[13] X. Yang, N. H. Thomas, L. J. Guo and Y. Hou, Two-way coupled bubble laden mixing layer, Chemical Engineering Science 57 (2002), 555-564.

[14] G.-H. Cottet and P. Koumoutsakos, Vortex Methods: Theory and Applications, Cambridge University Press, Cambridge, 2000.

[15] Y. Murai and Y. Matsumoto, Numerical analysis of detailed flow structures in bubble plume, 2nd report, three-dimensional flow structure and turbulence mechanism, JSME International Journal Ser. B 63 (1997), 2283-2288.

[16] D. W. Moore, The boundary layer on a spherical gas bubble, J. Fluid Mech. 16 (1963), 161-176.

[17] O. Caballina, E. Climent and J. Dušek, Two-way coupling simulations of instabilities in a plane bubble plume, Phys. Fluids 15 (2003), 1535-1544.